Magnetic and transport properties in metallic and disordered Ru2VAl and Ru2VGa

Sanchayita Mondal, Krishanu Ghosh, R. Ranganathan, Eric Alleno, Chandan Mazumdar

Magnetic and transport properties in metallic and disordered Ru_2VAl and Ru_2VGa

Sanchayita Mondal[a,b], Krishanu Ghosh[c], R. Ranganathan[b], Eric Alleno[d], Chandan Mazumdar[b,*]

[a] *Maharaja Manindra Chandra College, 20 Ramkanto Bose Street, Kolkata 700003, West Bengal, India*
[b] *Condensed Matter Physics Division, Saha Institute of Nuclear Physics, 1/AF, Bidhannagar, Kolkata 700064, India*
[c] *Department of Physics, P.C. Vigyan College, Kathari Bag Road, Chapra, 841301, Bihar, India*
[d] *Univ Paris Est Creteil, CNRS, ICMPE, UMR 7182, 2-8, rue H. Dunant, F-94320 THIAIS, France*

Abstract

In this work, we report an elaborate study on the structural, magnetic and thermoelectric properties of two Ru-based Heusler alloys, *viz.*, Ru_2VAl and Ru_2VGa, having valence electron count 24. While Ru_2VGa exhibits a nonmagnetic ground state, in Ru_2VAl a short range ferromagnetic interaction is developed below 10 K due to the structural antisite defects and disorder, that also manifests its signature in the specific heat and electrical resistivity measurements at low temperatures. Both the Seebeck coefficient (S) and Hall measurements suggest the dominance of hole-type carrier for electronic transport in Ru_2VAl whereas Ru_2VGa is found to be a n-type material. The linear nature and small absolute values of S, as well as non-zero values of electronic contribution to specific heat γ_S ($\gamma_{S\,Ru_2VAl}$ = 4.9 mJ/mol-K^2 and $\gamma_{S\,Ru_2VGa}$ = 5.5 mJ/mol-K^2) point towards a metallic ground state for both these alloys. Both the compounds exhibit lower thermal conductivity at room temperature in comparison to Fe-based Heusler alloys due to the presence of heavier element Ru.

1. Introduction

More than a century after the discovery of ferromagnetism in Cu_2MnAl by Fritz Heusler in 1903, the investigation of the Heusler alloys still remains a field of active research as new and fascinating physical properties as well as their scope of technological applications, keep on emerging at regular intervals [1, 2, 3]. Interestingly, by only variation of their valence electron count (VEC) per formula unit, the alloys of this family show variety of magnetic and transport phenomenon, such as half-metallic ferromagnetism, magneto-optical properties, semimetallic/semiconducting behaviour, *etc.*, that make them suitable for different practical applications, *viz.*, spintronics, magnetic memory devices, thermoelectricity... [3, 4, 5, 6, 7, 8, 9]. The Heusler compounds having VEC 24 are generally found to be semimetallic/semiconducting as well as non-magnetic due to the Slater-Pauling rule which assumes that the total magnetic moment per unit cell (M) of an ordered Heusler alloy would be M (μ_B) = |VEC–24| [10]. Having a semiconducting or semimetallic ground state with a narrow gap or pseudogap in the vicinity of the Fermi level (E_F) these compounds have drawn intense interests towards the optimization of their thermoelectric properties for practical applications [11, 12, 13]. Among the few most elaborately studied compounds of this class, stoichiometric and perfectly ordered Fe_2VAl and Fe_2VGa are indeed found to be non-magnetic semimetal/semiconductor by extensive theoretical and experimental works [11, 12]. In some cases, nevertheless, a weak magnetic behaviour has been reported in Heusler alloys with VEC = 24, *e.g.*, Fe_2VAl, Fe_2VGa, Fe_2TiSn, *etc.* [14, 15, 16, 17, 18], whose origin has been attributed to the inherent presence of structural antisite defects and disorders.

*Corresponding author
Email address: chandan.mazumdar@saha.ac.in (Chandan Mazumdar)

It is often noticed that these type of disorders not only have profound influence on magnetic properties but the transport properties, specially resistivity (ρ), thermopower (S), as well as the thermal conductivity (κ) may also be affected by such disorders [18, 19, 20, 21]. It has been reported that the presence of antisite defects in Fe_2VAl often help to enhance thermoelectric figure-of-merit (ZT, defined as $S^2T/\rho\kappa$) by decreasing lattice thermal conductivity while simultaneously improving the power factor (PF, defined as S^2/ρ) [22, 23]. It should be mentioned here that low thermal conductivity as well as large thermopower are desired to achieve a good thermoelectric material as the efficiency of a thermoelectric device depends upon the ZT of the thermoelectric materials.

Till date, quite a few Heusler compounds having VEC 24, namely, Fe_2VAl, Fe_2VGa and other Fe-based alloys have been synthesized and studied in order to find good thermoelectric materials. As Ru and Fe have similar outermost electronic configurations, some Ru-based Heusler compounds have been recently added to this family. Ru_2NbAl, Ru_2NbGa and Ru_2TaAl exhibit semimetallic ground state and a value of ZT $\sim$ 5.2 $\times$ 10^{-3} at 300 K, relatively larger than that of Fe-based compounds, has been found in Ru_2NbAl [24, 25, 26]. Similar to some of the Fe-based compounds having VEC = 24, presence of superparamagnetism as well as ferromagnetically correlated clusters have been reported in Ru_2NbAl as well [24]. Through the study of structural, electronic and thermoelectric properties of Ru_2VAl and Ru_2VGa, it was found that both the compounds display weak metallic behaviour with low residual resistivity ratio [27, 28, 29, 30, 31]. At 300 K a n-type Seebeck coefficient of absolute value -13.3 μV/K has been reported in Ru_2VAl whereas in Ru_2VGa it is found to be positive $\sim$ 8.5 μV/K [29]. These values are somewhat lower than the corresponding Fe-based Heusler compounds. However, on close inspection, one may find some inconsistencies in the thermal conductivity values reported for these two alloys. It is well known that in a compound, fully substituting an element by a heavier isoelectronic one leads to a decrease of the lattice thermal conductivity (κ_L) due to a smaller Debye temperature and speed of sound [32]: for instance κ_L in Fe_2VAl is 28 W/m-K at 300 K whereas it is 19 W/m-K in Fe_2VGa [33, 34, 35, 36, 37, 38, 39]. The same rule applies in half-Heusler compounds MNiSn, where κ_L is 15 and 10 W/m-K for M = Zr and Hf respectively [40, 41]. However, the reported value of κ_L at 300 K in Ru_2VAl (8 W/m-K) is surprisingly smaller than in Ru_2VGa (12 W/m-K) [29]. Another effect which can influence the lattice thermal conductivity is crystallographic site disorder such as the above-mentioned antisite defects: the engendered on-site mass fluctuation leads to "Rayleigh" scattering of the heat carrying phonons and to a decrease of the lattice thermal conductivity. Ru_2VAl is indeed reported to crystallize in a disordered B2 structure in ref.[31] but reported in the ordered $L2_1$ structure in ref.[29]. Ru_2VGa is reported in the ordered $L2_1$ structure in both references [29, 31] but may display a significative degree of crystalline disorder as well. Magnetism, which has not yet been explored, and the electronic transport properties can also be influenced by the structural disorder, which certainly occurs in these two compounds. We therefore decided to re-examine in the present work these questions. It will be underlined that both compounds grossly display the same transport and magnetic properties but that the observed differences indeed arise from Ru_2VAl being more strongly disordered than Ru_2VGa.

2. Experimental details

The sample ingots were prepared by arc melting stoichiometric amounts of the constituting elements on a water-cooled copper hearth in a flowing Ar atmosphere. To promote homogeneity, the ingots were flipped over and melted several times. The weight losses of the resultant materials were found to be less than 0.5%. The as-cast ingots were then annealed in an evacuated quartz tube at 1273 K for 48 hours and quenched in ice-water. After cleaning the scrap from the surface, the samples were annealed again at 1223 K for 12 hours. Then the ingots were cut in appropriate shapes and annealed again for 2 hours at 1173 K followed by quenching in ice-water. Similar post-synthesis sample treatments were earlier reported in Fe_2VAl [42] and Ru_2NbAl [24] to eliminate any kind of surface strain or "cold work" that may have been generated during cutting and polishing the samples. The phases content as well as the crystal structure were investigated using powder X-ray diffraction (XRD). Room temperature diffraction was carried out with a Brucker D8 diffractometer (Cu K_α) whereas temperature-dependent measurements were carried out between 300–12 K using a diffractometer associated with a rotating Cu Kα anode operated

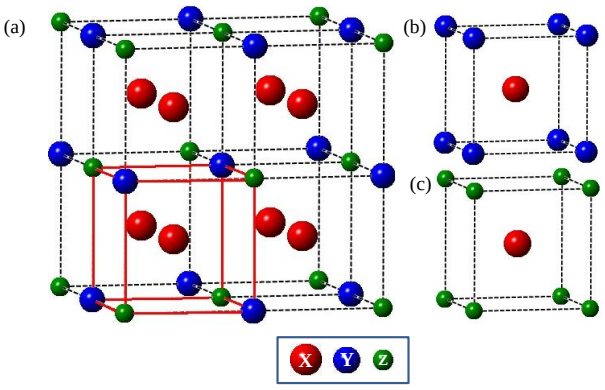

Figure 1: (a) The Heusler structure X_2YZ corresponding $L2_1$ structure, (b) and (c) CsCl-type or B2 disorder.

at 9 kW power [Model: TTREX III, M/s Rigaku Corp., Japan]. The Rietveld refinement technique was implemented using FullProf software [43] for the analysis of the XRD patterns. The wavelength dispersive spectroscopy based electron probe microanalysis (EPMA) technique [Model: SX 100, Cameca, France] was used to determine the chemical compositions and microstructure of the annealed alloys. Magnetization [M (T, H)], thermal transport [ρ(T), S(T), κ(T)], Hall coefficient [R_H(T)] and heat capacity [C(T)] were measured using commercial set ups [Models: SQUID-VSM and PPMS Evercool-II, M/s Quantum Design Inc., USA].

3. Results and Discussion

3.1. Structural and microstructural details

In order to get a clear picture of the properties of a Heusler alloy an elaborate study of the crystal structure is crucial. The most ordered structure for a Heusler compound X_2YZ is $L2_1$ (space group $Fm\bar{3}m$) containing four interpenetrating *fcc* sublattices (Fig. 1(a)), where X atoms occupy two of them having the 8c Wyckoff positions ($\frac{1}{4}\frac{1}{4}\frac{1}{4}$) and ($\frac{3}{4}\frac{3}{4}\frac{3}{4}$) and the Y and Z atoms are located at the other two *fcc* sublattices 4b ($\frac{1}{2}\frac{1}{2}\frac{1}{2}$) and 4$a$ (0 0 0), respectively [3, 44]. Unit cell of the $L2_1$ structure can also be easily seen as eight *bcc* unit cells stacked together to form a *fcc* structure where all the body center sites are occupied by the X atoms and the corner sites are occupied by Y and Z atoms alternatively. It is often noticed that depending upon their synthesis procedure and heat treatment, these compounds are not formed in a completely ordered structure and exhibit various degree of disorder [18, 19, 21]. If the Y and Z atoms exchange their positions and are randomly distributed over all the corner sites of the *bcc* lattices, then these positions become equivalent and the crystal structure remains with only eight simple *bcc* unit cells, corner sites of which are irregularly occupied by Y (Fig. 1(b)) or Z (Fig. 1(c)) atoms irregularly with X atoms at center sites. This resulting structure is often known as a CsCl-type or B2-type structure. As a consequence, the space group becomes $Pm\bar{3}m$ and the lattice parameters of the $L2_1$ and B2 phases are related by $a_{L2_1} = 2a_{B2}$. In any cases, XRD analysis can distinguish between these two structures. For the $L2_1$ structure, the allowed Bragg reflections are those for which Miller indices are either all odd or all even whereas in the B2 phase reflections for only all even h, k, l appear. Thus, the $L2_1$ phase can be uniquely identified by the occurrence of *fcc*-typical all odd reflections *i.e.*, (111), (311) *etc.*, and the absence of these peaks can be interpreted as the occurrence of only the B2 phase. However, it often becomes difficult to distinguish between $L2_1$ and B2 phases when the intensity of the all odd reflections are very low, particularly when the atomic numbers of the constituent elements of a Heusler compound are similar, the intensity of these peaks can be below 1% of the most intense (220) reflection [45]. The intensity of the (111) superlattice reflection depends on the crystal structure factor F_{111}, related to the atomic scattering factors as $F_{111} \propto (f_Y\text{-}f_Z)$, where f_Y and f_Z are the atomic scattering factors of the Y and Z atoms respectively [46].

For better understanding of the present experimental XRD data, we have calculated the powdered XRD patterns for Ru_2VAl and Ru_2VGa considering both $L2_1$ and B2 structures using FullProf software with a constant scale factor. It has been found that the intensity of the (111) peak is 2% of the most intense (220) line for Ru_2VAl (Fig. 2) whereas it is only 1% in case of Ru_2VGa (Fig. 3). Experimentally observed as well as calculated room-temperature XRD patterns considering both $L2_1$ and B2 structures of polycrystalline Ru_2VAl and Ru_2VGa are shown in Fig. 2 and 3. An extra line with a small intensity at $\sim 37^\circ$ is observed in the XRD patterns for both of these compounds, similar to that often reported in many Ru based Heusler alloys and assigned to a Ru-rich phase [24, 25, 26, 31]. All the other diffraction lines could be indexed within the B2

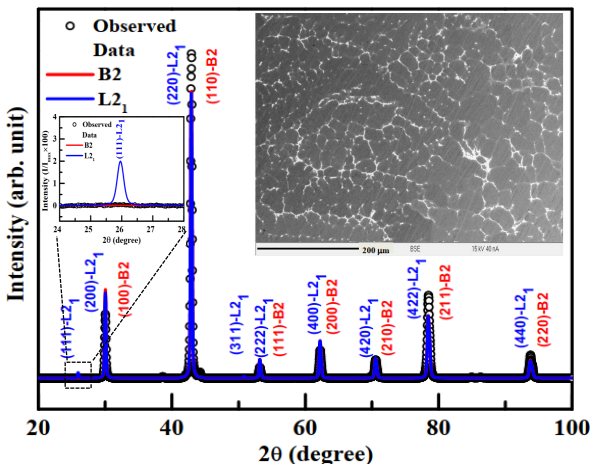

Figure 2: Experimentally observed XRD pattern of Ru_2VAl at room temperature along with calculated XRD patterns using Fullprof software considering both B2 and $L2_1$ structure; Inset: (left) an enhanced picture of the (111)-$L2_1$ peak, (right) back scattered image.

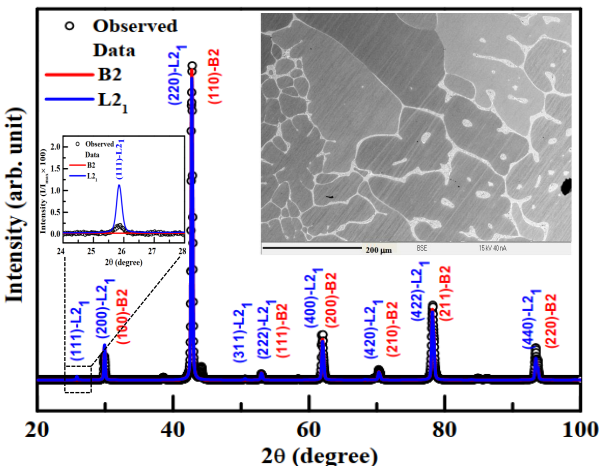

Figure 3: The room temperature XRD pattern of Ru_2VGa along with generated XRD patterns corresponding both B2 and $L2_1$ structure; Inset: (left) an enlargement of the (111)-$L2_1$ reflection, (right) back scattered image

structure for Ru_2VAl whereas Ru_2VGa crystallizes in the $L2_1$ structure. Indeed, a close scrutiny of the XRD patterns at the lower diffraction angles reveals that the *fcc*-typical (111) and (311) reflections do not appear in the XRD patterns of Ru_2VAl while the occurrence, despite its small intensity, in the Ru_2VGa pattern of a (111) line is an unambiguous proof of its $L2_1$ structure. The Rietveld refinement confirmed the simple analysis discussed above. While for the former compound, the lattice parameter and site occupancies are estimated to be 2.9887(1) Å and $Ru_{1.95}V_{0.98}Al_{1.09}$, they are 5.9927(2) Å and $Ru_{1.93}V_{1.14}Ga_{0.94}$ for the latter compound. The reduced intensity of (111) peak in the XRD pattern of Ru_2VGa suggests that the system most likely forms with a partially disordered structure, as indicated by the non-stoichiometric composition estimated from the Rietveld analysis. In case of Ru_2VAl, the extent of disorder is much higher, resulting in a system that completely forms in B2-type structure.

The Electron Probe Micro-Analysis was also used to determine the microstructure in the Ru_2VAl and Ru_2VGa samples. Backscattered electron images (Insets of Fig. 2 & Fig. 3) show for both the samples a main phase with 30±10 μm and 15–150 μm grains respectively, surrounded by a uniform layer of secondary phases distributed at the boundaries. This morphology is typical of a solidified main phase coexisting with a eutectic, solidifying at a lower temperature when cooling. The chemical compositions, measured at 60 points of the sample, are found to be $Ru_2V_{0.9\pm0.1}Al_{1.1\pm0.1}$ and $Ru_{1.95}V_{1.16\pm0.02}Ga_{0.89\pm0.01}$ for the main phase respectively. The broad range of compositions and the B2 disordered structure observed for Ru_2VAl are consistent with the existence of a solid solution between RuV (B2) and RuAl (B2), as already reported by Povarova *et al.* [47]. On the other hand, despite its non-stoichiometry, the narrower range of compositions as well as its ordered $L2_1$ structure are characteristic of Ru_2VGa being a compound with a narrower range of homogeneity in the ternary phases diagram. For both Ru_2VAl and Ru_2VGa, deviations from stoichiometry are observed in their EPMA compositions, in agreement with the XRD analysis. These deviations from stoichiometry lead to the occurrence of secondary phases, balancing the actual compositions of the main phases. The eutectic $Ru_{72}V_{28}$ + $V_{50}Ru_{50}$ [48] is thus found in the Ru_2VAl sample at the grain boundaries. The averaged composition $Ru_{59}V_{26}Ga_{15}$ is observed at the grain boundaries in Ru_2VGa but the absence of a Ru-Ga binary phases diagram prevents any safe assignment to known eutectics. In Ru_2VAl, the B2 structure implies that Ru occupies a single crystalline site whereas V and Al are fully mixed on the same shared site, giving rise to 0.5 V_{Al} and 0.5 Al_V antisite defects per formula unit (f.u.). Due to the deviation from stoichiometry, these

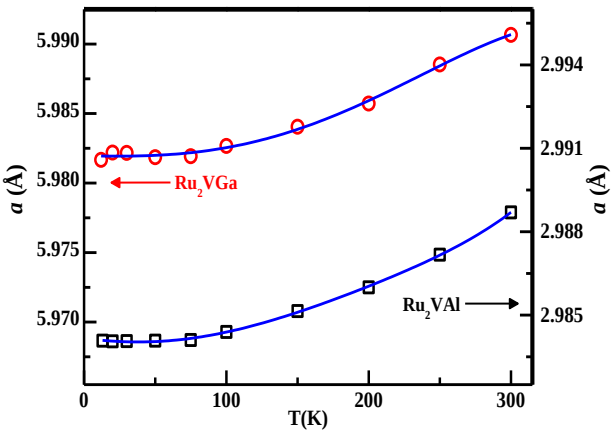

Figure 4: Temperature dependance of lattice parameter of Ru_2VAl and Ru_2VGa respectively along with fit to Eq. 1.

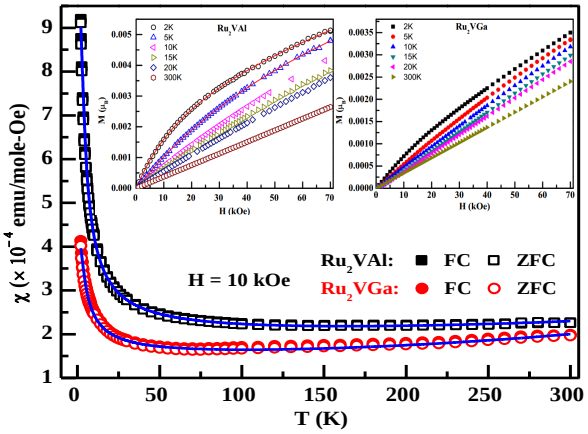

Figure 5: Temperature dependent magnetic susceptibility of Ru_2VAl and Ru_2VGa, measured at 10 kOe externally applied magnetic field under ZFC configuration, The solid lines are the fit to Eq.3. Inset: Isothermal magnetization data at various temperature for (a) Ru_2VAl and (b) Ru_2VGa. The solid lines represent the fit using Eq.4.

concentrations are corrected to 0.45 V_{Al} and 0.55 Al_V per f.u.. Similarly, for Ru_2VGa crystallizing in the $L2_1$ structure, the deviation from stoichiometry leads to 0.05 V_{Al} and 0.03 V_{Ru} per f.u.. The influence of these defects on the thermal, magnetic and transport properties will be further discussed.

To check for the possibility of any structural change at any lower temperatures, XRD data have been collected down to 12 K for both Ru_2VAl and Ru_2VGa. The analysis of the low temperature XRD data, suggests that the crystal structure remains unaltered for both the samples. As the temperature decreases, the lattice parameter decreases gradually. The temperature dependance of lattice parameters of Ru_2VAl and Ru_2VGa are plotted and fitted (Fig. 4) with the equation

$$V(T) = \gamma_G U(T)/K_0 + V_0, \qquad (1)$$

where V_0 is the cell volume at T = 0 K, K_0 is the bulk modulus, and γ_G is the Grüneisen parameter. *U(T)* is the internal energy, which can be expressed according to the Debye approximation as

$$U(T) = 9NK_BT\left(\frac{T}{\Theta_D}\right)^3 \int_0^{\frac{\Theta_D}{T}} \frac{x^3}{e^x - 1}dx \qquad (2)$$

where N is the number of atoms per unit cell. The estimated Debye temperatures and Grüneisen parameters are Θ_D = 510 K and γ_G = 2.2 for Ru_2VAl and Θ_D = 370 K and γ_G = 1.6 for Ru_2VGa, respectively. In order to estimate the Grüneisen parameters, theoretically calculated values of K_0 of Ru_2VAl (239 GPa) and Ru_2VGa (241 GPa) [30] have been used. The Θ_D value is lower in Ru_2VGa due to the heavier atomic mass of Ga than that of Al.

3.2. Magnetic properties

3.2.1. Magnetic susceptibility

The dc magnetic behaviour of both Ru_2VAl and Ru_2VGa have been investigated at externally applied magnetic fields, H = 10 kOe and H = 70 kOe. The temperature dependent susceptibility (χ(T)) curves do not show any thermoremanent behaviour between zero field cooled (ZFC) and field cooled (FC) conditions (Fig. 5), down to the lowest measured temperature, 2 K. In spite of having upturns in the χ(T) curves at low temperatures, the values of χ remain almost invariant over a wide temperature range for both of these materials. The small magnitude as well as the absence of any peak (or saturation in the low temperature region) in the magnetic susceptibilities of these two materials suggest that both are primarily paramagnetic in nature. However, the χ(T)) curves do not follow the well-known paramagnetic Curie-Weiss behaviour, suggesting the presence of additional Pauli paramagnetic contribution for both the alloys. The χ(T) curves could be described very well with a modified Curie-Weiss law [49]

$$\chi(T) = \frac{C}{T - \theta_p} + \chi_0 + \alpha T^2, \qquad (3)$$

The first term is the standard Curie-Weiss expression, where, $C = \frac{N_A \mu_{eff}^2 \mu_B^2}{3k_B}$, is the Curie constant, μ_{eff} is the paramegnetic moment in units of Bohr magnetons μ_B, N_A is the Avogadro's number and k_B is Boltzmann's constant. χ_0 is the temperature-independent term that includes the diamagnetic or Pauli paramagnetic contributions and the last term αT^2 is considered to be originating from the higher order temperature dependent contribution in the Pauli paramagnetism, which is usually neglected in the zero-order approximation [49]. The values of the parameters extracted from the fit of χ(T) for H = 10 kOe for both the samples are listed in Table 1. The values of χ_0 and α are found of the same order as earlier reported values in Ru_2NbAl [24] and $SrIrO_3$ [49]. The small value of μ_{eff} in Ru_2VGa is reminiscent of its non-magnetic behaviour, predicted by the Slater-Pauling law. The slightly larger non-zero values of μ_{eff} and θ_p found in Ru_2VAl is likely to arise from its more disordered structure. Nonetheless, they should not result from the 0.45 V_{Al} and 0.55 Al_V per f.u. antisite defects unveiled by the structural/microstructural analysis. Their concentrations is indeed orders of magnitude larger than the concentration of atomic magnetic moments that could produce the small magnetic response hereby measured. The relationship between the magnetic response of Ru_2VAl and its defects will be further discussed through isothermal magnetization.

Table 1: Parameters (χ_0, θ_p and α) extracted from the fit of χ(T) for H = 10 kOe to Eq.3 for both Ru_2VAl and Ru_2VGa. The μ_{eff}s are calculated using the values of C.

	χ_0 (emu/mol-Oe)	μ_{eff} (μ_B)	θ_p (K)	α (emu/mol-Oe-K^2)
Ru_2VAl	1.9×10^{-4}	0.15	−1.8	3.1×10^{-10}
Ru_2VGa	1.5×10^{-4}	0.09	−2.4	5.1×10^{-10}

3.2.2. Isothermal magnetization

The variation of magnetization as a function of externally applied field, M(H), studied at different temperatures for both Ru_2VAl and Ru_2VGa are shown in Fig. 5(a) and 5(b), respectively. At room temperature, for both the compounds, the M(H) curves exhibit a linear behaviour, whereas a small downward curvature start to manifest with decrease in temperature. The linear nature of isothermal magnetization can be found in both paramagnetic (PM) as well as antiferromagnetic (AFM) systems. Since the magnetic susceptibility in the temperature range 300–2 K can be explained by considering paramagnetic ground state, the possibility of any AFM ordering at higher temperature (T>300 K) can be ruled out. Further, the magnetic susceptibilities of both the compounds do not show any anomaly indicating the signature of any long range magnetic order in the temperature range 300–2 K. However, the M(H) curve of both the compounds start to exhibit deviation from linearity with decrease in temperature. While the deviation appear to be barely discernible for Ru_2VGa (Fig. 5(b)), whereas the deviation is more signifiacant, particularly below 15 K, in case of Ru_2VAl (Fig. 5(a)). The non-linear nature of the isothermal magnetization curves gradually gets stronger as the measuring temperature is reduced to 5 K and 2 K. The magnetization at 2 K evolves towards a saturation-like behaviour but does not show any hysteresis (Fig. 5(a)). Such S-shaped anhysteretic M(H) curve can originate in short range interactions since the χ(T) behaviour of Ru_2VAl has already ruled out the possibility of any long range ordering throughout the investigated temperature range. Similar M(H) behaviour was earlier reported in isostructural Ru_2NbAl, Fe_2VAl and other Fe-based Heusler alloys due to the presence of superparamagnetically interacting clusters [14, 24, 50]. Ferromagnetic (FM) interactions among clusters were also found to have grown at lower temperatures for some of those compounds [14, 24, 50].

In order to investigate the exact nature of the short range interactions in Ru_2VAl, we have analyzed the magnetization curves taken at 2 K and 5 K considering a superparamagnetic (SPM) state. To assert SPM for a compound experimentally, two conditions must be satisfied. Firstly, the anhysteretic M(H) curves taken at different temperatures must be described by the Langevin function separately and secondly, if these isotherms are plotted as a function of H/T, they must fall on a single curve [51]. Here we have used a modified Langevin function considering both SPM and PM phases, represented by

$$M(H) = M_S L(x) + \chi H \tag{4}$$

where $x = \frac{\mu H}{k_B T}$, M_S is the saturation

magnetization, μ is the average magnetic moment per cluster, and $L(x) = coth(x) - 1/x$ is the Langevin function. The $M_S L(x)$ term represents the SPM component, whereas the χH represents the paramagnetic contribution. Though we get a reasonably good fit for both the temperatures, the curves do not fall on the universal curve of reduced magnetization (M/M_S) as a function of H/T. Non-fulfillment of all the criterion for SPM thus ruled out the possibility of presence of superparamagnetically interacting clusters in Ru_2VAl and rather point towards the occurrence of ferromagnetic interaction. In Ru_2NbAl, Fe_2VAl *etc.*, the origin of the FM interaction was argued to be the random anisotropy arising from the structural antisite defects [14, 24, 50]. To find the nature of the interactions in Ru_2VAl, we have used the random anisotropy (RA) model [52] to analyze the M(H) data for T$\leq$5 K. In this model, the magnetic ground state of materials having different strength of random anisotropy for a large range of experimentally applied magnetic fields, has been calculated. A variety of magnetic ground states can be identified depending upon the strength of applied field (H) in comparison to the parameter H_s, where $H_s = H_r^4/H_{ex}^3$ with H_r and H_{ex} are the anisotropic field and exchange field, respectively. In low field regime, (H<H_s), one can find a correlated spin glass that shows large susceptibility. For the intermediate-field strength, H_s<H<H_{ex}, the spins of the system are nearly aligned along the applied field direction. However, the magnetization direction of locally correlated regions varies due to the random anisotropy present in the system. This state is called the "ferromagnet with wandering axis (FWA)". In this regime, the magnetization approaches toward saturation as

$$M(H) = M_s^{FM}\left[1 - \frac{1}{15}\left(\frac{H_s}{H}\right)^{\frac{1}{2}}\right] \qquad (5)$$

where M_s^{FM} is the saturation magnetization. If the effect of coherent anisotropy is also considered, then H can be replaced by $(H+H_c)$ in Eq.5 for a field H>H_c, where H_c is the field due to the coherence portion of the anisotropy. In such case, M would gradually approach towards M_s as

$$M(H) = M_s^{FM}\left[1 - \frac{1}{15}\left(\frac{H_s}{H + H_c}\right)^{\frac{1}{2}}\right]. \qquad (6)$$

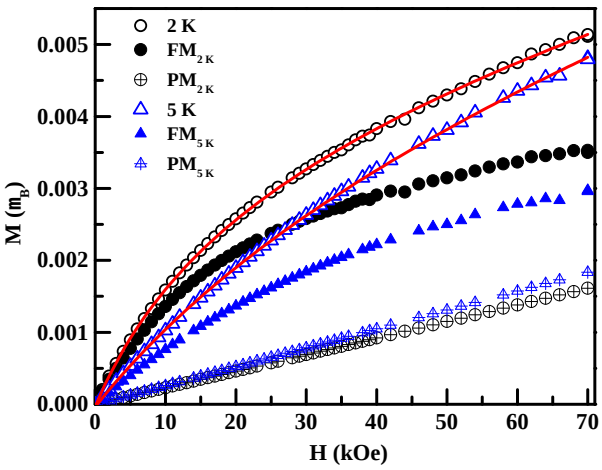

Figure 6: Isothermal magnetization data at 5 K and 2 K for Ru_2VAl along with fit (solid line) to the Eq.7 + χH and the FM and PM contributions of the same isothermals.

It may be noted here that the usage of the prefactor 1/15 in Eq.6, originally calculated for $H_r << H_{ex}$[52], can be applied only when the magnetization has reached over (1-$\frac{1}{15}$)% *i.e.* 93% of its saturation value [53]. In the present case, the saturation value of M(H) at 2 K and at 70 kOe field appears to be substantially lower. As a result, using the 1/15 prefactor is unlikely to be appropriate in our system and therefore requires a suitable correction. A similar situation in case of $Dy_xY_{1-x}Al_2$ [53], $GdAl_2$[54], $Co_{58.5}Ga_{41.5}$[55] and Ru_2NbAl [24] had earlier been dealt by considering the prefactor of the order of 1. Accordingly, by using a prefactor equal to unity, Eq.6 is modified to

$$M(H) = M_s^{FM}\left[1 - \left(\frac{H_s}{H + H_c}\right)^{\frac{1}{2}}\right] \qquad (7)$$

Excellent fits are achieved for the M(H) data (Fig. 6) at 5 K and 2 K using Eq.7 with an additional paramagnetic term χH. The parameters extracted from the fits of 5 K and 2 K magnetic isotherms are listed in Table 2. The random anisotropy field H_s and H_c are found to be comparable to each other. The values of H_s for both the temperatures are found to be less than the maximum applied field (70 kOe) and thus fulfills the condition H>H_s. As any of the values of H_r or H_{ex} is not known to us, we can not estimate the anisotropy strength in Ru_2VAl from the values of H_s. However, this analysis suggests the presence of ferromagnetically correlated regions (clusters) in Ru_2VAl. The magnetization directions of these

Table 2: Parameters extracted from the fit of M(H) curves for 2 and 5 K to Eq.7 + χH for Ru_2VAl.

	M_s^{FM} (μ_B/f.u.)	H_s (kOe)	H_c (kOe)	χ (μ_B/kOe-f.u.)
2 K	0.0060(2)	14.7(6)	14.6(6)	$2.3(1)\times10^{-5}$
5 K	0.0074(1)	38.7(7)	38.4(7)	$2.6(1)\times10^{-5}$

clusters are pinned or frozen by random anisotropy, as found in case a correlated glassy system.

3.3. Heat capacity

To verify the magnetic analysis for Ru_2VAl and Ru_2VGa, we have measured specific heat, C(T), in the temperature range 2-300 K for both compounds (Fig. 7). The C(T) curves do not show any peak for both the samples, confirming the absence of long range magnetic order as earlier suggested by the magnetic susceptibility measurements.

Usually, the heat capacity for a metal in the paramagnetic region can be described by the well known Debye model [56], expressed as

$$C(T) = \gamma_S T + 9nR\left(\frac{T}{\Theta_D}\right)^3 \int_0^{\frac{\Theta_D}{T}} \frac{x^4 e^x}{(e^x-1)^2} dx \quad (8)$$

where, the electronic specific heat is represented by the first term and lattice/phonon contribution comes from the second term. The Sommerfeld coefficient, γ_S, is equal to $\frac{1}{3}\pi^2 D(E_F) {k_B}^2$, where $D(E_F)$ stands for the density of states at the Fermi level E_F. n and Θ_D are the number of atoms per formula unit (For Ru_2VZ, Z = Al, Ga: n = 4) and the Debye temperature, respectively, and $x = \hbar\omega/k_B T$. The standard Debye model, can well explain the C(T) data from 300 K to 10 K and yields Θ_D=444 K for Ru_2VAl and Θ_D=390 K for Ru_2VGa, respectively. While the value of Θ_D, found for Ru_2VGa is consistent with that of the value estimated from the fit of the lattice parameter vs temperature curve, it is found to be little lower in case of Ru_2VAl. This fit of the high temperature C(T) data also yielded $\gamma_S \sim 10$ mJ/mol-K^2 for both compounds, a value inaccurate and incompatible with the low temperature C(T)/T vs T^2 data shown in the inset of Fig. 7 where $\gamma_S \sim 5$ mJ/mol-K^2 is expected in both cases. To accurately estimate γ_S, a simplified form of Eq.8 was implemented:

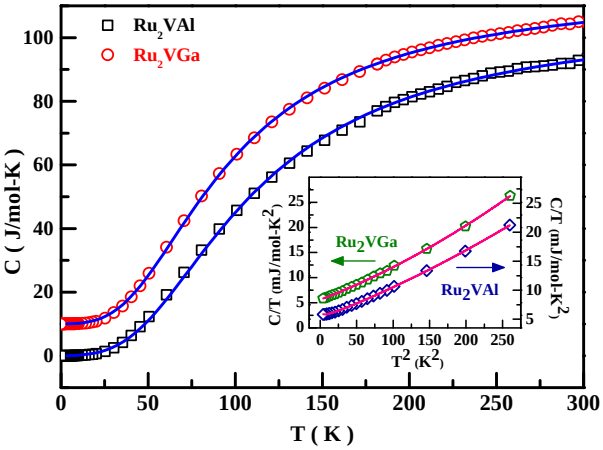

Figure 7: Specific heat as a function of temperature of Ru_2VZ, (Z = Al, Ga): to avoid the cluttering of the two curves, the data of Ru_2VGa presented here has been shifted up by adding a constant value of 10 J/mol-K to the original data; Inset: C/T vs T^2 plot at low temperature for both Ru_2VAl and Ru_2VGa.

$$C(T) = \gamma_S T + \beta T^3 + \delta T^5 + \cdots\cdots \quad (9)$$

where, β, δ *etc.* are the coefficients. At a temperature T$\leq \Theta_D/50$, Eq.9 is generally expressed as $C(T) = \gamma_S T + \beta T^3$ after ignoring T^5 and other higher order terms and thus C/T vs T^2 plot becomes linear having a slope $\beta = (12\pi^4/5) N k_B/{\Theta_D}^3$ [56]. However, C/T vs T^2 curve for Ru_2VAl is not linear below 5 K (Fig. 7; Inset). It can be mentioned here that isothermal magnetic measurements of Ru_2VAl indicate the development of ferromagnetic clusters below 5 K. Therefore, the non-linear nature in C/T vs T^2 curve of Ru_2VAl points towards the presence of inter/intra-clusters magnetic interactions.

Similar deviation in C(T) curve in low temperature has also been reported for Fe_2VAl [57], Ru_2NbAl [24], V-Fe [58], Ti-Fe alloy [59] and the reason behind this behaviour was ascribed to oscillations of small FM clusters. The compounds having ferromagnetic clusters are usually kept in a position of minimum energy in nonferromagnetic matrix and if a force is able to alter the direction of the magnetization vector of these clusters, then the potential energy of these compounds is increased. This excess energy is usually stored in local elastic deformation of the clusters as well as in magnetostriction energy [59]. Hence, due to thermal perturbation, a $k_B T$ amount of energy is absorbed by each cluster to oscillate

about the mean position determined by the crystal anisotropy energy. This contributes an extra term $C_0 \sim 2k_BN$ to total specific heat for N number of oscillating magnetic clusters [59, 58]. However, according to the third law of thermodynamics, the heat capacity must be zero at T = 0 K. To satisfy this law, C_0 becomes weaker slowly below a particular temperature, called Einstein temperature, $T_E = 2\mu_B H/k_B$, where H is the required magnetic field that produces the same amount of torque as produced by the crystal anisotropy energy. Generally in most of the compounds $T_E < 1$ K [58, 60]. After inclusion of the cluster interaction term C_0, Eq.9 is transformed to

$$C(T) = \gamma_S T + \beta T^3 + \delta T^5 + C_0 + \cdots\cdots \quad (10)$$

Eq.10 matches well with experimentally observed data of specific heat for Ru_2VAl in the range $2 \leq T \leq 20$ K. In Eq.10, δT^5 term has been included to fit the temperature region, $T > \Theta_D/50$. It may be noted here that we have used Eq.10 for both the compounds, Ru_2VAl and Ru_2VGa (Fig. 7; Inset) to compare the values of C_0 and confirm the presence of magnetic cluster in Ru_2VAl. The estimated values of the parameters from this fit are given in Table 3. Using the value of C_0 we have calculated the number of ferromagnetic clusters (N). On the one hand, an almost negligible value of N in Ru_2VGa agrees with its paramagnetic behaviour confirmed earlier by the magnetization measurements. On the other hand, in consistency with its deviation from paramagnetism below 5 K, $N \sim 5.4 \times 10^{19}$ ferromagnetic clusters per mol are found in Ru_2VAl . In our previous work on Ru_2NbAl [24], these clusters had been related to antisite defects. Nonetheless, the number of clusters $N \sim 5.4 \times 10^{19}$ per mol is several orders of magnitude smaller than the number of V_{Al} and Al_V antisite defects ($\sim 0.5 \times 6.02 \times 10^{23} = 3 \times 10^{23}$ defects per mol) detected by XRD and EPMA. Moreover, since V_{Al} and Al_V are reported to be non-magnetic in Fe_2VAl [61, 62], they cannot be considered as responsible for the weak magnetic behaviour of Ru_2VAl. Thus, in analogy with Fe_2VAl [61, 62] and Ru_2NbAl [24], we surmise that the ferromagnetic clusters could be identified with $5.4 \times 10^{19} / 6.02 \times 10^{23} = 9 \times 10^{-5}$ mol per (f.u.) of Ru_V or Ru_{Al} defects, undetected by EPMA.

Table 3: The estimated parameters from the fit of C/T versus T^2 curves to Eq. 10 for both Ru_2VAl and Ru_2VGa.

	γ_S (mJ/ mol-K^2)	β (mJ/ mol-K^4)	δ (mJ/ mol-K^6)	C_0 (mJ/ mol-K)
Ru_2VAl	4.9	0.049	4.83×10^{-5}	1.5
Ru_2VGa	5.5	0.057	8.64×10^{-5}	0.2

3.4. Transport

3.4.1. Resistivity

Fig. 8 shows the temperature dependent electrical resistivity $\rho(T)$ in Ru_2VAl and Ru_2VGa. For both the samples $\rho(T)$ curves exhibit positive temperature coefficient of resistivity (TCR) suggesting a metallic ground state, in agreement with a previous report [29]. The value of resistivity at room temperature (ρ_{300K}) and residual resistivity ratio (RRR) for Ru_2VAl are 350 $\mu\Omega$-cm and $\sim$1.08, respectively, in Ru_2VGa, ρ_{300K} is found to be 265 $\mu\Omega$-cm and RRR = 1.2. Although the nature of the $\rho(T)$ curves is metallic, low value of RRR and relatively large ρ_{300K} categorize both these compounds as bad metal. An upturn at low temperature (below 50–70 K) can nonetheless be observed in the $\rho(T)$ curve of Ru_2VAl (Fig. 8). The metallic part of the $\rho(T)$ data could be modelled to electron-phonon interaction in the frame work of the Boltzmann transport theory using Bloch-Grüneisen formula [63] as follows:

$$\rho(T) = \rho_0 + \rho(\Theta_D)\left(\frac{T}{\Theta_D}\right)^5 \int_0^{\frac{\Theta_D}{T}} \frac{x^5}{(e^x - 1)(1 - e^{-x})} dx \quad (11)$$

where, $\rho(\Theta_D)$ and ρ_0 are the values of resistivity at the Debye temperature and at 0 K. The $\rho(T)$ curve for Ru_2VGa is very well fitted using the above equation. The parameters extracted from the fit are $\Theta_D = 367$ K, $\rho(\Theta_D) = 55$ $\mu\Omega$-cm and $\rho_0 = 221$ $\mu\Omega$-cm. The resistivity behaviour of Ru_2VAl can not be described by Eq. 11 in the whole temperature range, as the upturn in low temperatures indicates the presence of an additional contribution. It may be recalled here that the XRD and EPMA have shown the presence of large concentration of antisite defects: 0.45 V_{Al} and 0.55 Al_V per f.u. Such disorder often results in a charge carrier localization [64], which can be modelled by the variable range

hopping (VRH) mechanism proposed by Mott [65]. In this mechanism, electrons hop to energetically close and localized states and the conduction law of VRH can be expressed as:

$$\rho(T) = \rho_0 + Aexp\left[\left(\frac{T_0}{T}\right)^{1/4}\right] \qquad (12)$$

where A is a constant and T_0 is the activation temperature that depends on the localization length (ξ) as ξ^{-3} [65]. The $\rho(T)$ curve for Ru_2VAl can be well explained by using Eq. 11 and Eq. 12 together. The fitted parameters extracted are Θ_D = 526 K, $\rho(\Theta_D)$ = 51 $\mu\Omega$-cm, ρ_0 = 315 $\mu\Omega$-cm and A = 5.3 $\mu\Omega$-cm. The values of Θ_D, estimated for Ru_2VAl from lattice thermal expansion and resistivity measurements are found to be higher than that of the value extracted from the heat capacity. However, the values of Θ_D calculated from all these three measurements are in agreement for Ru_2VGa. It should be mentioned here that the Debye temperature evaluated from heat capacity usually differ from the Θ_D, obtained by electrical resistivity measurement because only longitudinal phonons have been considered in the theory to develop Bloch-Grüneisen formula [66]. The agreement between Θ_Ds, found from heat capacity and lattice thermal expansion are generally observed at high temperatures. However, in some cases, consistencies are also reported between all these three Θ_D values [66, 67]. The difference in the $\rho(T)$ data between Ru_2VAl and Ru_2VGa can thus be ascribed to the more disordered character of the crystal structure in the former compound (B2) than in the latter ($L2_1$).

3.4.2. Seebeck coefficient

The Seebeck coefficient (S) was measured in the temperature range 2-300 K for both Ru_2VAl and Ru_2VGa, as shown in Fig. 9. The S(T) curve of Ru_2VAl remains positive, suggesting that the dominant carriers for the electronic transport are holes in this compound. The absolute value of S is found to be only 3 μV/K at 300 K and decreases when temperature decreases towards a zero value at 0 K. These small values are typical of a metallic ground state. The positive value of S(T) in Ru_2VAl is related to the deviation from stoichiometry giving a larger number of Al_V electron acceptors than of V_{Al} electron donor antisite defects [68]. A non-linear behaviour below 150 K (Fig. 9(I)) arising from an extra contribution can also be seen in

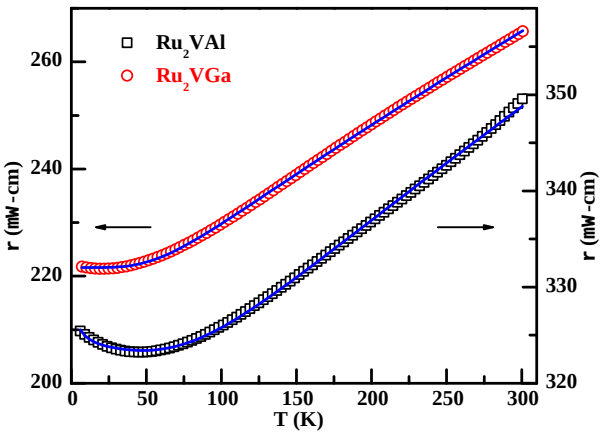

Figure 8: Resistivity as a function of temperature for Ru_2VZ.

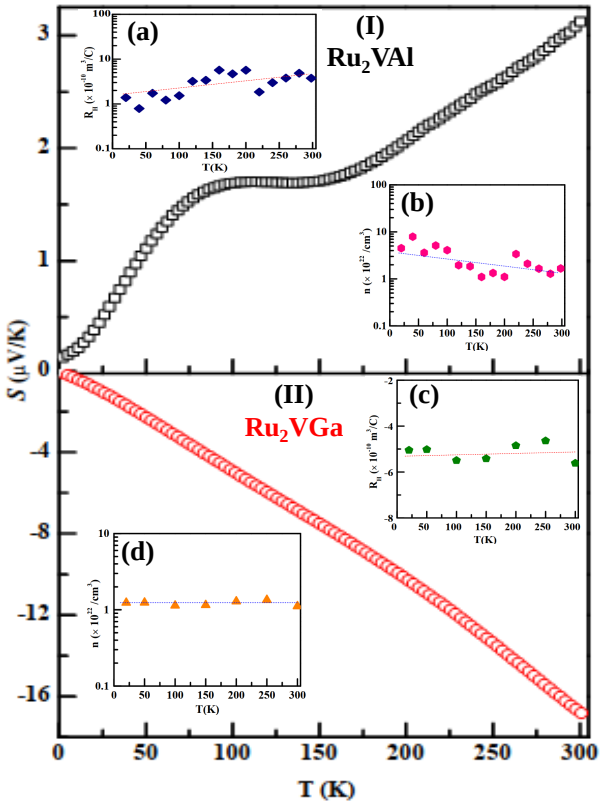

Figure 9: Temperature dependance of Seebeck coefficient of (I) Ru_2VAl and (II) Ru_2VGa; Inset: (a) and (c) Hall coefficient of Ru_2VAl and Ru_2VGa respectively, (b) The hole concentration of Ru_2VAl, and (d) The electron concentration of Ru_2VGa.

S(T). This could be related to phonon drag but a more probable explanation could reside in the localization visible in the resistivity upturn below ∼

100 K (Fig. 8): a small imbalance between hole and electron localization could give rise to the observed extra contribution [69]. For Ru_2VGa, the S(T) curve shows only negative values. It decreases nearly linearly with temperature from zero at 0 K to -16.6 μV/K at 300 K (Fig. 9(II)). This variation is also typical of a metallic state in line with the occurrence of 0.05 f.u.$^{-1}$ V_{Al} electron donor antisite defects. Although the measurements on different batches of samples resulted in slightly different values in S(T), the sign remained unaltered for all the 9 batches in both the compounds. In the present work, large differences are noticed in the S(T) behaviour for both Ru_2VAl and Ru_2VGa than their earlier reported result [29], particularly in the sign of S. In earlier work [29], the S(T) curve of Ru_2VAl showed linear behaviour and was negative throughout the temperature range up to 300 K. The value of S at 300 K was -13.3 μV/K for Ru_2VAl whereas in Ru_2VGa it was found to be positive $\sim$8.5 μV/K at 300 K and remained positive in the whole temperature range. Discarding the possibility of unintentional switching of samples, one may note that the different heat treatment as well as small deviation in the chemical composition could also be the possible reason behind the differing S(T) behaviour in Ru_2VAl and Ru_2VGa.

3.4.3. Hall coefficient

In order to ensure the veracity of the signs of our experimentally observed Seebeck coefficient data, another independent experimental probe, the Hall coefficient (R_H) measurements were carried out on both Ru_2VAl and Ru_2VGa in the temperature range 20-300 K applying an external applied magnetic field of 50 kOe. For Ru_2VAl, the magnitude of R_H remains positive throughout the temperature region examined (Fig. 9; inset(a)) suggesting the dominance of hole-type carrier in electronic transport in conformity with the positive sign of S observed in this compound (Fig. 9; (I)). On the other hand, the negative value of R_H in Ru_2VGa (Fig. 9; inset(c)) confirms the fact that the majority carriers are electrons for Ru_2VGa (Fig. 9; (II)), which is also inferred earlier in this work through the Seebeck coefficient measurements. Irrespective of the sign for both Ru_2VAl and Ru_2VGa, the magnitude of observed R_H is found to be $\sim 10^{-10}$ m^3/C, which is similar to that of a typical metal. The effective carrier concentrations(n) are calculated using the relation $n = 1/eR_H$, where e is the elementary charge of the electron. The magnitude of R_H as well as the hole and electron concentrations in Ru_2VAl and Ru_2VGa respectively remain almost constant (Fig. 9; inset(c)&(d)) in the entire temperature range, extrapolating to large non-zero values ($> 10^{22}$ cm^{-3}) at 0 K. Both the Hall and Seebeck coefficient data are thus strongly in agreement with the metallic ground state suggested by the electrical conductivity measurements for both these two compounds.

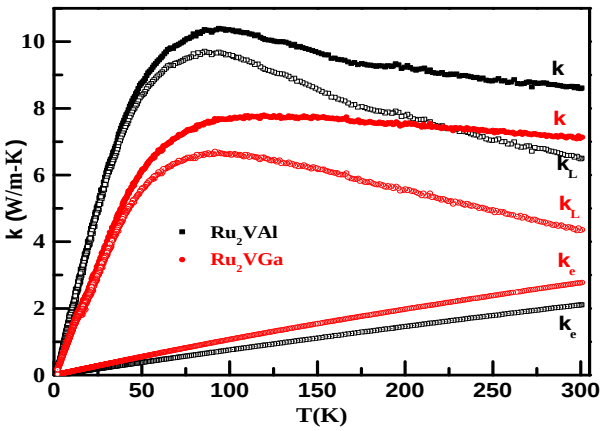

Figure 10: Temperature variations of the total thermal conductivity κ, lattice thermal conductivity κ_L, and electronic thermal conductivity κ_e for Ru_2VZ,(Z = Al, Ga) as a function of temperature.

3.4.4. Thermal conductivity

Fig. 10 shows the thermal conductivity (κ), measured between 2-300 K. For ordinary metals, the total thermal conductivity is a sum of electronic (κ_e) and lattice (κ_L) terms. The electronic thermal conductivity can be evaluated using the Wiedemann-Franz law $\kappa_e\rho$/T = L_0, where ρ is the measured dc electric resistivity and $L_0 = 2.45\times10^{-8}$ WΩK^{-2} is the Lorenz number. The lattice thermal conductivity κ_L can thus be obtained by subtracting κ_e from the observed κ and it is also plotted in Fig. 10. The overall variations with temperature of κ_L in both compounds are typical of crystalline materials where phonon scattering by electron or grain boundaries dominates the very low temperature portion, mass fluctuation or Rayleigh scattering dominates the intermediate temperature range and phonon-phonon scattering affects the "high" temperature one [32]. The values of κ_L at room temperature are found to be 6.5 and 4.5 W/m-K for Ru_2VAl and Ru_2VGa, respectively. Noticeably, the observed value of κ_L in Ru_2VGa is

lower than that of Ru_2VAl. Similar to the mismatch in the S(T) behaviour of Ru_2VAl and Ru_2VGa between the present and an earlier reported work [29], noticeable differences are observed in the κ_L(T) behaviour also for both the compounds. In the earlier report, the values of κ_L in Ru_2VGa were found to be higher (12 W/mK at 300 K) than that of in Ru_2VAl (8 W/m-K at 300 K) [29]. Occurrence of lower κ_L values in a compound containing element of comparably lower atomic mass is usually not observed in Heusler alloys as well as in other thermoelectric materials. If one of the constituent elements of any of these compounds is substituted with an isoelectronic heavier element, it is found that the value of κ_L gets reduced in that alloy having heavier element [24, 25, 26, 33, 34, 35, 36, 37, 38, 39, 40, 41]. Moreover, the Debye temperature (see section 3.4.1) and the speed of sound, both reflecting the lattice dynamics in these compounds, are larger in Ru_2VAl [30] than in Ru_2VGa. In view of these facts, it can be concluded that the present value of κ and κ_L for Ru_2VAl and Ru_2VGa are more consistent with the general trend reported among Heusler alloys and other compounds.

The κ_L values of Ru_2VAl and Ru_2VGa at 300 K are much lower than those in Fe_2VAl ($\sim$ 28 W/m-K) and Fe_2VGa ($\sim$ 17 W/m-K) [35, 36, 37, 38]. The reduction in κ_L values in Ru-based alloys in comparison to Fe-based alloys are anticipated as ruthenium is heavier than iron. Further decrease in κ_L values may be attributed to the structural antisite disorders [70, 71] present in Ru_2VAl. The structural antisite defects and disorders generally diminish κ_L in the intermediate temperature range by introducing point defects in the lattice [72, 73]. Nonetheless, despite their small values of κ, as will be further discussed, the metallic ground state in Ru_2VAl and Ru_2VGa currently prevents any possibility of a large ZT in these two compounds.

3.4.5. Figure of merit

The dimensionless figure of merit of Ru_2VAl and Ru_2VGa is plotted versus temperature and displayed in Fig. 11. The largest value is reached in both compounds at 300 K: it is $ZT = 10^{-4}$ and $ZT = 4.4\times10^{-3}$ in Ru_2VAl and Ru_2VGa, respectively. These values are order of magnitude smaller than in Bi_2Te_3, the reference compound displaying $ZT \sim 1$ [74] at 300 K. For practical thermoelectric applications, the value of ZT of a thermoelectric material needs to be equals to or greater than one.

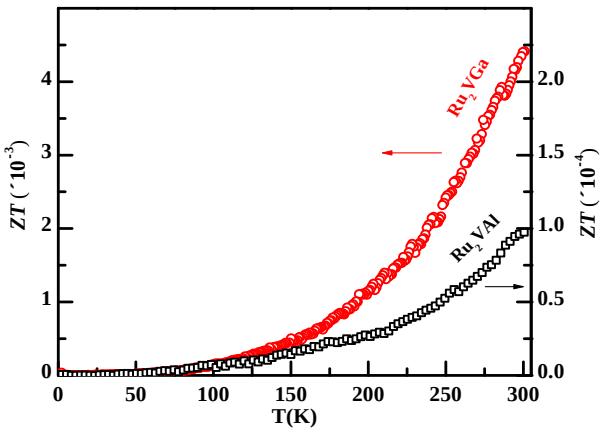

Figure 11: ZT value as a function of temperature for Ru_2VZ, (Z = Al, Ga).

In order to obtain such large figure of merit, not only the κ should be low, but the power factor (PF=S^2/ρ) should be quite high as well. The effective strategy that is generally followed by the researchers to optimize these thermoelectric parameters is by tuning the electronic density of states through partial/full doping or substitution of foreign elements at different crystallographic sites. It should be noted here that many such efforts have been made to optimize the thermoelectric properties of Fe_2VAl, resulting in an encouraging increment in the Seebeck coefficient value from $\sim$35 μV/K to $\sim$130 μV/K [14, 34, 35, 36, 39]. In Ru_2TaAl and Ru_2NbGa, by introducing off-stoichiometry, substantial increase in ZT could be achieved [26, 75]. As already discussed, both Ru_2VAl and Ru_2VGa although show low values of thermal conductivity, a 10 to 100 times smaller Seebeck coefficient than the typical values found in well established doped Heusler materials ($\sim \pm$ 130 μV/K) remain a big deterrent. Accordingly, one may expect a many-fold increase in the magnitude of S, by tuning the ground state of Ru_2VAl and Ru_2VGa from metal-like to semiconductor-like through appropriate doping or elemental substitution without compromising the low thermal conductivity characteristic of these materials.

4. Conclusion

Structural, magnetic and thermoelectric properties of Ru-based Heusler alloys Ru_2VAl

and Ru_2VGa have extensively been studied. Ru_2VGa is found to be nonmagnetic as expected for a Heusler compound having VEC 24 whereas in Ru_2VAl a short-range ferromagnetic interaction is developed below 10 K. This deviation from the nonmagnetic behaviour is attributed to the structural antisite defects. B2 disorder is also manifested in the specific heat as well as electrical transport properties at low temperatures. The Seebeck coefficient as well as Hall measurements reveal that Ru_2VAl is a p-type material whereas the majority carrier for transport is electrons in Ru_2VGa. The mismatch in the sign of charge carrier between the earlier published results and our study has been explained through different sample compositions, where we have ignored the possibility of unintentional switching of samples in the earlier published work. The small values of S, the hole/electron concentration $\sim 10^{22}$ in Ru_2VAl/Ru_2VGa as well as non-zero values of γ_S ($\gamma_{SRu_2VAl} = 4.9$ mJ/mol-K^2 and $\gamma_{SRu_2VGa} = 5.5$ mJ/mol-K^2) suggest a metallic ground state for both theses alloys. Both of these compounds exhibit lower thermal conductivity at room temperature vis-à-vis the earlier reported values. Additionally, our observation of larger value of κ in Ru_2VAl in comparison to Ru_2VGa is in agreement with the fact that Ga has greater atomic weight than Al. Although these undoped compounds may not be very useful for practical thermoelectric application due to their relatively small ZT values and their metallic ground states, they show a huge potential for a many-fold enhancement of the Seebeck coefficient, and consequently the figure of merit by appropriately tuning their density of states through suitable doping/substitution, similar to that reported for Fe_2VAl in literature.

5. Acknowledgment

We thank Prof. G. Vaitheeswaran, University of Hyderabad for useful discussion during the earlier stage of this work.

References

[1] F. Heusler, Magnetic manganese alloys, Verhandl Deuts Phys Ges 5 (1903) 219.

[2] F. Heusler, W. Starck, E. Haupt, Magnetisch-chemische studien, Verh. Dtsch. Phys. Ges 5 (1903) 219–232.

[3] T. Graf, C. Felser, S. S. Parkin, Simple rules for the understanding of heusler compounds, Progress in solid state chemistry 39 (1) (2011) 1–50 and references there in.

[4] C. Felser, G. H. Fecher, B. Balke, Spintronics: a challenge for materials science and solid-state chemistry, Angewandte Chemie International Edition 46 (5) (2007) 668–699.

[5] P. Van Engen, K. Buschow, R. Jongebreur, M. Erman, PtMnSb, a material with very high magneto-optical Kerr effect, Applied Physics Letters 42 (2) (1983) 202–204.

[6] T. Krenke, E. Duman, M. Acet, E. F. Wassermann, X. Moya, L. Mañosa, A. Planes, Inverse magnetocaloric effect in ferromagnetic Ni–Mn–Sn alloys, Nature materials 4 (6) (2005) 450–454.

[7] R. Kainuma, Y. Imano, W. Ito, Y. Sutou, H. Morito, S. Okamoto, O. Kitakami, K. Oikawa, A. Fujita, T. Kanomata, et al., Magnetic-field-induced shape recovery by reverse phase transformation, Nature 439 (7079) (2006) 957–960.

[8] S. Wurmehl, G. H. Fecher, H. C. Kandpal, V. Ksenofontov, C. Felser, H.-J. Lin, Investigation of Co_2FeSi: The Heusler compound with highest Curie temperature and magnetic moment, Applied physics letters 88 (3) (2006) 032503.

[9] W. Wang, E. Liu, M. Kodzuka, H. Sukegawa, M. Wojcik, E. Jedryka, G. Wu, K. Inomata, S. Mitani, K. Hono, Coherent tunneling and giant tunneling magnetoresistance in Co_2 FeAl/MgO/CoFe magnetic tunneling junctions, Physical Review B 81 (14) (2010) 140402.

[10] I. Galanakis, P. Dederichs, N. Papanikolaou, Slater-Pauling behavior and origin of the half-metallicity of the full-Heusler alloys, Physical Review B 66 (17) (2002) 174429.

[11] Y. Nishino, M. Kato, S. Asano, K. Soda, M. Hayasaki, U. Mizutani, Semiconductorlike behavior of electrical resistivity in Heusler-type Fe_2VAl compound, Physical review letters 79 (10) (1997) 1909.

[12] A. Ślebarski, J. Goraus, Electronic structure and thermodynamic properties of Fe_2VGa, Physical Review B 80 (23) (2009) 235121.

[13] A. Ślebarski, J. Deniszczyk, W. Borgieł, A. Jezierski, M. Swatek, A. Winiarska, M. Maple, W. Yuhasz, Electronic structure and thermodynamic properties of the Heusler alloys $Fe_2Ti_{1-x}V_xSn$, Physical Review B 69 (15) (2004) 155118.

[14] M. Vasundhara, V. Srinivas, V. Rao, Evidence for cluster glass behavior in Fe_2 VAl Heusler alloys, Physical Review B 78 (6) (2008) 064401.

[15] C.-S. Lue, J. H. Ross Jr, C. Chang, H. Yang, Field-dependent specific heat in Fe_2VAl and the question of possible 3 d Heavy Fermion behavior, Physical Review B 60 (20) (1999) R13941.

[16] C. Lue, Y. Li, J. H. Ross Jr, G. M. Irwin, NMR and Mössbauer study of spin dynamics and electronic structure of $Fe_{2+x}V_{1-x}Al$ and Fe_2VGa, Physical Review B 67 (22) (2003) 224425.

[17] A. Matsushita, Y. Yamada, Physical properties of Heusler-type Fe_2VA1 compound, Journal of magnetism and magnetic materials 196 (1999) 669–670.

[18] Y. Feng, J. Rhee, T. Wiener, D. W. Lynch, B. Hubbard, A. Sievers, D. Schlagel, T. Lograsso, L. Miller, Physical properties of heusle-like Fe_2VAl, Physical Review B 63 (16) (2001) 165109.

[19] A. Abhyankar, Y. Yu, Y. Kuo, G. Huang, C. Lue,

Thermal and transport properties of $Ni_2MnGa_{1-x}Al_x$ alloys, Intermetallics 18 (11) (2010) 2090–2095.
[20] Y. Nishino, H. Sumi, U. Mizutani, Transport and magnetic properties of the Heusler-type $Fe_{2-x}V_{1+x}Al$ system ($-$ 0.01$\leq$ x$\leq$ 0.08), Physical Review B 71 (9) (2005) 094425.
[21] R. Umetsu, K. Kobayashi, A. Fujita, R. Kainuma, K. Ishida, Magnetic properties and stability of $L2_1$ and B2 phases in the Co_2MnAl heusler alloy, Journal of Applied Physics 103 (7) (2008) 07D718.
[22] S. Bandaru, A. Katre, J. Carrete, N. Mingo, P. Jund, Influence of antisite defects on the thermoelectric properties of Fe_2VAl, Nanoscale and Microscale Thermophysical Engineering 21 (4) (2017) 237–246.
[23] T. Nakama, Y. Takaesu, K. Yagasaki, T. Naka, A. Matsushita, K. Fukuda, Y. Yamada, Transport properties of Heusler compounds $Fe_{3-x}V_xAl$, Journal of the Physical Society of Japan 74 (5) (2005) 1378–1381.
[24] S. Mondal, C. Mazumdar, R. Ranganathan, E. Alleno, P. Sreeparvathy, V. Kanchana, G. Vaitheeswaran, Ferromagnetically correlated clusters in semimetallic Ru_2NbAl Heusler alloy and its thermoelectric properties, Physical Review B 98 (20) (2018) 205130.
[25] C. Kuo, H. Lee, C.-M. Wei, Y. Lin, Y. Kuo, C. Lue, Ru_2NbGa: A Heusler-type compound with semimetallic characteristics, Physical Review B 94 (20) (2016) 205116.
[26] C. Tseng, C. Kuo, H. Lee, K. Chen, R. Huang, C.-M. Wei, Y. Kuo, C. Lue, Semimetallic behavior in Heusler-type Ru_2TaAl and thermoelectric performance improved by off-stoichiometry, Physical Review B 96 (12) (2017) 125106.
[27] S. Mondal, C. Mazumdar, R. Ranganathan, Structural and transport properties of two new Heusler type Ru_2VAl and Ru_2VGa compounds, in: AIP Conference Proceedings, Vol. 1512, American Institute of Physics, 2013, pp. 978–979.
[28] S. Mondal, C. Mazumdar, R. Ranganathan, Ru_2VAl and Ru_2VGa: Two new heusler-type compounds, in: AIP Conference Proceedings, Vol. 1536, American Institute of Physics, 2013, pp. 825–826.
[29] B. Ramachandran, Y. Lin, Y. Kuo, C. Kuo, A. Gippius, C. Lue, Thermoelectric properties of Heusler-type $Ru_2VAl_{1-x}Ga_x$ alloys, Intermetallics 92 (2018) 36–41.
[30] H. Abbassa, S. Hadjri-Mebarki, B. Amrani, T. Belaroussi, K. D. Khodja, P. Aubert, Theoretical investigation of new Heusler alloys $Ru_2VGa_{1-x}Al_x$, Journal of Alloys and Compounds 637 (2015) 557–563.
[31] M. Yin, P. Nash, Standard enthalpies of formation of selected Ru_2YZ Heusler compounds, Journal of Alloys and Compounds 634 (2015) 70–74.
[32] J. Yang, Theory of thermal conductivity, in: Thermal conductivity, Springer, 2004, pp. 1–20.
[33] Y. Xia, S. Bhattacharya, V. Ponnambalam, A. Pope, S. Poon, T. Tritt, Thermoelectric properties of semimetallic (Zr, Hf) CoSb half-Heusler phases, Journal of applied physics 88 (4) (2000) 1952–1955.
[34] Y. Nishino, H. Kato, M. Kato, U. Mizutani, Effect of off-stoichiometry on the transport properties of the Heusler-type F_2VAl compound, Physical Review B 63 (23) (2001) 233303.
[35] C.-S. Lue, Y.-K. Kuo, Thermoelectric properties of the semimetallic Heusler compounds $Fe_{2-x}V_{1+x}M$ (M= Al, Ga), Physical Review B 66 (8) (2002) 085121.
[36] Y. Nishino, S. Deguchi, U. Mizutani, Thermal and transport properties of the Heusler-type $Fe_2VAl_{1-x}Ge_x$ (0$\leq$ x$\leq$0.20) alloys: Effect of doping on lattice thermal conductivity, electrical resistivity, and Seebeck coefficient, Physical Review B 74 (11) (2006) 115115.
[37] C.-S. Lue, W. Lai, C. Chen, Y. Kuo, Off-stoichiometric effect on the transport and pseudogap characteristics of Fe_2VGa, Journal of Physics: Condensed Matter 16 (24) (2004) 4283.
[38] C.-S. Lue, J. Huang, D. Tsai, K. Sivakumar, Y. Kuo, Effects of Ge substitution on the thermoelectric properties and pseudogap characteristics of Fe_2VGa, Journal of Physics: Condensed Matter 20 (25) (2008) 255233.
[39] M. Vasundhara, V. Srinivas, V. Rao, Low-temperature electrical transport in Heusler-type $Fe_2V(AlSi)$ alloys, Journal of Physics: Condensed Matter 17 (38) (2005) 6025.
[40] C. Uher, J. Yang, S. Hu, D. Morelli, G. Meisner, Transport properties of pure and doped MNiSn (M= Zr, Hf), Physical Review B 59 (13) (1999) 8615.
[41] H. Hohl, A. P. Ramirez, C. Goldmann, G. Ernst, B. Wölfing, E. Bucher, Efficient dopants for ZrNiSn-based thermoelectric materials, Journal of Physics: Condensed Matter 11 (7) (1999) 1697.
[42] S. Maier, S. Denis, S. Adam, J.-C. Crivello, J.-M. Joubert, E. Alleno, Order-disorder transitions in the Fe_2VAl Heusler alloy, Acta Materialia 121 (2016) 126–136.
[43] J. Rodríguez-Carvajal, Recent advances in magnetic structure determination by neutron powder diffraction, Physica B: Condensed Matter 192 (1-2) (1993) 55–69.
[44] O. Heusler, Crystal structure and the iron magnetism of manganese-aluminium-copper alloys, Ann. Phys 19 (1934) 155–201.
[45] T. Gasi, V. Ksenofontov, J. Kiss, S. Chadov, A. Nayak, M. Nicklas, J. Winterlik, M. Schwall, P. Klaer, P. Adler, et al., Iron-based Heusler compounds Fe_2YZ: Comparison with theoretical predictions of the crystal structure and magnetic properties, Physical Review B 87 (6) (2013) 064411.
[46] A. J. Bradley, J. Rodgers, The crystal structure of the Heusler alloys, Proceedings of the royal society of london. Series A, Containing Papers of a Mathematical and Physical Character 144 (852) (1934) 340–359.
[47] K. Povarova, N. Kazanskaya, A. Drozdov, O. Skachkov, Refractory intermetallic compound RuAl as a basis of less-traditional superalloys, Russian Metallurgy (Metally) (3) (2002) 235–245.
[48] F. Aldinger, A. F. Guillermet, V. S. Iorich, L. Kaufman, W. A. Oates, H. Ohtani, M. Rand, M. Schalin, Group 6: periodic systems effects, Calphad: Computer Coupling of Phase Diagrams and Thermochemistry 19 (4) (1995) 555–571.
[49] P. E. Blanchard, E. Reynolds, B. J. Kennedy, J. A. Kimpton, M. Avdeev, A. A. Belik, Anomalous thermal expansion in orthorhombic perovskite $SrIrO_3$: Interplay between spin-orbit coupling and the crystal lattice, Physical Review B 89 (21) (2014) 214106.
[50] R. Saha, V. Srinivas, T. C. Rao, Evolution of ferromagneticlike order in $Fe_2V_{1-x}Cr_xAl$ Heusler alloys, Physical Review B 79 (17) (2009) 174423.
[51] C. Hurd, Varieties of magnetic order in solids, Contemporary Physics 23 (5) (1982) 469–493.
[52] E. Chudnovsky, W. Saslow, R. Serota, Ordering in

ferromagnets with random anisotropy, Physical Review B 33 (1) (1986) 251.
[53] P. Gehring, M. Salamon, A. Del Moral, J. Arnaudas, Magnetic static and scaling properties of the weak random-axis magnet $(Dy_xY_{1-x})Al_2$, Physical Review B 41 (13) (1990) 9134.
[54] P. Shand, C. Stark, D. Williams, M. Morales, T. Pekarek, D. Leslie-Pelecky, Spin glass or random anisotropy?: The origin of magnetically glassy behavior in nanostructured $GdAl_2$, Journal of applied physics 97 (10) (2005) 10J505.
[55] S. M. Yasin, R. Saha, V. Srinivas, S. Kasiviswanathan, A. K. Nigam, Anomalous Magnetic and Electrical Transport Behavior in Intermetallic $Co_{58.5}Ga_{41.5}$, IEEE Transactions on Magnetics 51 (11) (2015) 1–4.
[56] C. Kittel, P. McEuen, P. McEuen, Introduction to solid state physics, Vol. 8, Wiley New York, 1996.
[57] S. Podgornykh, A. Svyazhin, E. Shreder, V. Marchenkov, V. Dyakina, Low-temperature electron properties of Heusler alloys Fe_2VAl and Fe_2CrAl: Effect of annealing, Journal of Experimental and Theoretical Physics 105 (1) (2007) 42–45.
[58] K. Schröder, Effect of Magnetic Clusters on the Specific Heat of Ni-Cu and Fe-V Alloys, Journal of applied Physics 32 (5) (1961) 880–882.
[59] K. Schröder, C. Cheng, Correlation of Low-Temperature Caloric and Magnetic Effects in TiFe, Journal of Applied Physics 31 (12) (1960) 2154–2155.
[60] D. Ohlendorf, E. Wicke, A. Obermann, Low temperature specific heat and magnetic properties of V/Fe and V/Fe/H alloys, Journal of Physics and Chemistry of Solids 40 (11) (1979) 849–856.
[61] D. I. Bilc, P. Ghosez, Electronic and thermoelectric properties of Fe_2VAl: the role of defects and disorder, Physical Review B 83 (20) (2011) 205204.
[62] D. Singh, I. Mazin, Electronic structure, local moments, and transport in Fe_2VAl, Physical Review B 57 (22) (1998) 14352.
[63] F. J. Blatt, Physics of electronic conduction in solids, McGraw-Hill, 1968.
[64] R. Kelekar, B. Clemens, Epitaxial growth of the Heusler alloy $Co_2Cr_{1-x}Fe_xAl$, Journal of applied physics 96 (1) (2004) 540–543.
[65] N. Mott, Conduction in glasses containing transition metal ions, Journal of Non-Crystalline Solids 1 (1) (1968) 1–17.
[66] E. Gopal, Specific Heats at Low Temperatures, Springer, 1966.
[67] R. Goetsch, V. Anand, A. Pandey, D. Johnston, Structural, thermal, magnetic, and electronic transport properties of the $LaNi_2(Ge_{1-x}P_x)_2$ system, Physical Review B 85 (5) (2012) 054517.
[68] S. Bandaru, P. Jund, Electronic structure of the Heusler compound Fe_2VAl and its point defects by ab initio calculations, physica status solidi (b) 254 (2) (2017) 1600441.
[69] K. Yamamoto, A. Aharony, O. Entin-Wohlman, N. Hatano, Thermoelectricity near Anderson localization transitions, Physical Review B 96 (15) (2017) 155201.
[70] M. Mikami, Y. Kinemuchi, K. Ozaki, Y. Terazawa, T. Takeuchi, Thermoelectric properties of tungsten-substituted HeuslerFe_2VAl alloy, Journal of Applied Physics 111 (9) (2012) 093710.
[71] S. H. Zaferani, R. Ghomashchi, D. Vashaee, Strategies for engineering phonon transport in Heusler thermoelectric compounds, Renewable and Sustainable Energy Reviews 112 (2019) 158–169.
[72] C. Wood, Materials for thermoelectric energy conversion, Reports on progress in physics 51 (4) (1988) 459.
[73] C. Wan, Y. Wang, N. Wang, W. Norimatsu, M. Kusunoki, K. Koumoto, Development of novel thermoelectric materials by reduction of lattice thermal conductivity, Science and Technology of Advanced Materials (2010).
[74] H. Goldsmid, Thermoelectric refrigeration, Springer, 2013.
[75] P. Bag, W. Liu, Y.-K. Kuo, C. Kuo, C. Lue, Thermoelectric properties of chemically substituted Heusler-type $Ru_{2-x}Nb_{1+x}Ga$ and $Ru_2NbGa_{1-x}M_x$ (M= In, Ge, and Sn) alloys, Journal of Alloys and Compounds 849 (2020) 156617.